Editors' Suggestion

Scattering between Minivalleys in Twisted Double Bilayer Graphene

Petar Tomić,[1,*] Peter Rickhaus,[1] Aitor Garcia-Ruiz,[3] Giulia Zheng,[1] Elías Portolés,[1] Vladimir Fal'ko,[3,4] Kenji Watanabe,[5] Takashi Taniguchi,[6] Klaus Ensslin,[1,2] Thomas Ihn,[1,2] and Folkert K. de Vries[1,†]

[1]*Laboratory for Solid State Physics, ETH Zürich, CH-8093 Zürich, Switzerland*
[2]*Quantum Center, ETH Zürich, CH-8093 Zürich, Switzerland*
[3]*National Graphene Institute, University of Manchester, Manchester M13 9PL, United Kingdom*
[4]*Henry Royce Institute for Advanced Materials, M13 9PL Manchester, United Kingdom*
[5]*Research Center for Functional Materials, National Institute for Materials Science, 1-1 Namiki, Tsukuba 305-0044, Japan*
[6]*International Center for Materials Nanoarchitectonics, National Institute for Materials Science, 1-1 Namiki, Tsukuba 305-0044, Japan*

(Received 14 June 2021; revised 29 November 2021; accepted 8 December 2021; published 4 February 2022)

A unique feature of the complex band structures of moiré materials is the presence of minivalleys, their hybridization, and scattering between them. Here, we investigate magnetotransport oscillations caused by scattering between minivalleys—a phenomenon analogous to magnetointersubband oscillations—in a twisted double bilayer graphene sample with a twist angle of 1.94°. We study and discuss the potential scattering mechanisms and find an electron-phonon mechanism and valley conserving scattering to be likely. Finally, we discuss the relevance of our findings for different materials and twist angles.

DOI: 10.1103/PhysRevLett.128.057702

Two-dimensional moiré materials are formed by stacking van der Waals materials such that the layers couple and an in-plane superlattice emerges. The superlattice formed depends on the twist (and lattice mismatch) between the layers. Graphene is a typical van der Waals material and has a honeycomb lattice build up from two hexagonal sublattices. The wave functions of the two valleys K and K' in reciprocal space are sublattice polarized at the Dirac point [1]. Similarly, for trigonal moiré lattices, such as twisted graphene [2,3], the wave functions of the minivalleys κ and κ' are polarized on the twisted layers when the interlayer coupling is weak. Even though this is a generic property of trigonal moiré lattices, little is known about the scattering of charge carriers between these minivalleys.

We focus on twisted graphene since recently a plethora of correlated states has been observed [4–10], and in view of these correlations, scattering in twisted graphene is a highly interesting topic. Specifically, we choose to work with twisted double bilayer graphene (TDBG) with weak coupling between the layers, because this offers excellent control over the minivalley occupation, and high quality electron transport. This system resembles that of a weakly coupled double quantum well, where the two minivalleys around κ and κ' play the roles of the two subbands. Since the wave functions of the minivalleys are mostly bilayer polarized, a dual gate geometry provides independent control over the density in the two minivalleys, and with that, their energetic alignment [11].

A common way to obtain the leading scattering mechanism is analyzing the temperature dependence of the electrical resistivity [12]. Measurements of the resistivity in magic-angle twisted bilayer graphene have shown a linear temperature dependence, suggestive of electron-phonon scattering [13,14] or strange metallic behavior [15,16]. As the scattering between minivalleys is not necessarily the leading scattering mechanism, we introduce a more targeted approach. When applying a magnetic field, Landau levels are formed in both minivalleys separately. The energetic (mis)alignment of the modulated densities of states in the two minivalleys leads to oscillations in the interminivalley scattering. This oscillating interminivalley scattering is reflected in electrical transport through an effect analogous to magneto intersubband oscillations (MISO) [17,18]. In the following, we will refer to these magneto interminivalley oscillations as MISO, since they encapsulate the same physical phenomenon. The method we present is transferable to other moiré materials with a well developed Landau level spectrum as well as control of the energetic alignment of the minivalleys.

Here, we report measurements of MISO in TDBG with a twist angle of 1.94° and investigate the interminivalley scattering in the regime of hole-like states ($n < 0$). We introduce the band structure and tunability of the TDBG device by analyzing its Shubnikov–de Haas oscillations (SdHO) as a function of density and displacement field. Then we investigate two regions where MISO are particularly pronounced. First, toward the Lifshitz transition [19], we study MISO as a function of temperature and displacement field and discuss the scattering mechanism. Second, at the onset of the second minivalley, we discuss implications of the underlying scattering mechanism based on the observed valley degeneracy lifting. Finally, we discuss the impact of our findings with regard to different materials and twist angles.

We fabricate a Hall bar device [Fig. 1(a)] from TDBG sandwiched between two hexagonal boron nitride layers.

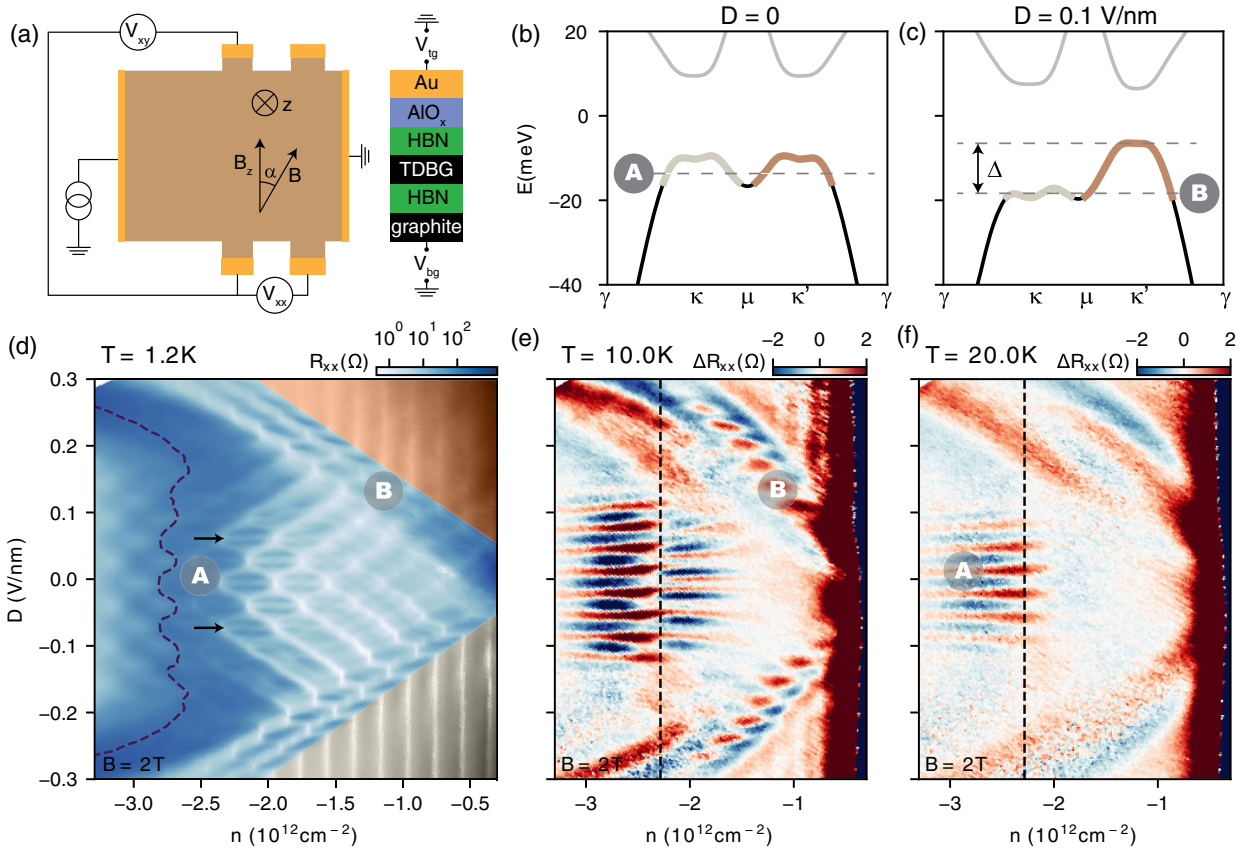

FIG. 1. (a) Schematic overview of the device, including setup to measure the longitudinal and Hall voltage (V_{xx} and V_{xy}), and an out-of-plane magnetic field B. Cross section of the device featuring the graphite, hexagonal boron nitride (HBN), TDBG, aluminium-oxide (AlO_x), and gold (Au) layers, and the top and bottom gates (V_{TG} and V_{BG}) indicated. (b),(c) Calculated band structure of TDBG (1.94°) for displacement field $D = 0$ and $D = 0.1$ V/nm, respectively. Minivalleys κ and κ' are indicated as well as the regions A and B. (d) R_{xx} as a function of density n and D at temperature $T = 1.2$ K and $B = 2$ T. Regions A and B are indicated. The overlayed colors bronze and gray indicate single minivalley regimes. The LT is highlighted by the dashed line. (e),(f) Resistance modulation $\Delta R_{xx}(n, D)$ at $B = 2$ T and $T = 10$ K and $T = 20$ K, respectively. The density used in Figs. 2 and 3 is indicated with a black dashed line.

A four-terminal current-bias setup is used to obtain the longitudinal resistance R_{xx} and Hall resistance R_{xy}, utilizing standard lock-in techniques with $I_{AC} = 100$ nA. Crucially, we are able to control the density n and displacement field D separately in the device through voltages applied to the top gate (V_{TG}) and bottom gate (V_{BG}) (see Supplemental Material [20]). We investigate the device in a ^{4}He cryostat with a base temperature of $T = 1.2$ K, and implemented temperature control. The device is identical to the one investigated in Ref. [27]. For details on the device fabrication and data analysis, see Supplemental Material [20].

The band structure of TDBG with a twist angle of 1.94° is presented in Fig. 1(b). The bands in the mini-Brillouin zone show local minima, maxima, and band gaps around the two minivalleys κ and κ'. Without an applied displacement field D the minivalleys are occupied equally (region A). In contrast, when a displacement field is applied, the energetic alignment of the minivalleys Δ is altered [11]. Independently tuning the Fermi energy now allows one to only occupy the bands centered around κ' [Fig. 1(c)], and reach asymmetric minivalley occupations (region B).

The tunability of our device with respect to the occupation of different minivalleys in the hole bands is investigated using SdHO. In Fig. 1(d) we show R_{xx} as a function of displacement field D and total density n measured at constant magnetic field $B = 2$ T and temperature $T = 1.2$ K. We observe a single set of SdHO in the regions masked with bronze and gray in Fig. 1(d), indicating the occupation of a single minivalley. This corresponds to the Fermi energy being tuned into the band gap of either minivalley [Fig. 1(c)]. The blue region in Fig. 1(d) corresponds to the configuration where both minivalleys κ and κ' are occupied, giving rise to a pattern of two sets of SdHO. Similar pattern has been observed due to interlayer Landau level pinning [26]. We reproduce this pattern within a simple model by considering screening effects of the bilayers as presented in Supplemental Material [20]. Finally, we highlight the Lifshitz transition [19] in Fig. 1(d) by drawing the contour (dashed line) where

$R_{xy} = 0$. At this line, the topology of the Fermi surface changes as the Fermi energy crosses the saddle point in the band structure at the μ point [see Figs. 1(b) and 1(c)] [11].

Interestingly, apart from the SdHO pattern, density independent resistance minima cutting through the middle of the hexagons are observed indicated with black arrows in the region labeled A in Fig. 1(d). Unlike SdHO, which are strongly thermally damped, these resistance minima are more pronounced at higher temperatures as seen at $T = 10$ K and $T = 20$ K in Figs. 1(e) and 1(f). There we plot the resistance modulation ΔR_{xx}, where we extracted a smooth background (R_{xx}^{BG}) using the Savitsky-Golay filter [30] and subtracted this from the data (R_{xx}): $\Delta R_{xx} = R_{xx} - R_{xx}^{\mathrm{BG}}$ (see Supplemental Material [20]). These oscillations are MISO [17,18], caused by an oscillating interminivalley scattering rate. The displacement field tunes the energy offset between the minivalleys, Δ [indicated in Fig. 1(c)] that periodically changes the energetic alignment of the Landau levels in the minivalleys. This results in a periodic modulation of the interminivalley scattering rate that we observe as MISO in Figs. 1(d)–1(f).

The unprecedented tunability of our TDBG device allows us to study MISO at various possible relative energetic alignments of the minivalleys. In particular, we observe enhanced MISO in two distinct regions denoted A and B in Figs. 1(d) and 1(f). Region A is located toward the Lifshitz transition for moderate values of displacement fields, and region B at the onset of the second minivalley.

We start discussing region A showing unambiguously the difference between MISO and SdHO. Line traces of R_{xx} as a function of D measured at different temperatures and constant density $n = -2.28 \times 10^2$ cm^{-2} (data measured at $n = -2.78 \times 10^{12}$ cm^{-2} is in Supplemental Material [20]) are shown in Fig. 2(a) revealing the suppression of SdHO with temperature, while MISO persist. At $T = 20$ K, as in Fig. 1(f), only MISO are left, whereas at $T = 1.2$ K, as in Fig. 1(d), SdHO are dominant and MISO are slightly visible as well. However, in the intermediate temperature regime, $T = 10$ K, the oscillations are commensurate. In Fig. 1(e), this leads to an apparent phase shift in MISO because with increasing density there is a shift around $n = -2.28 \times 10^{12}$ cm^{-2} from commensurate SdH and MISO regime to MISO dominated regime (see Supplemental Material [20]).

In order to show that the oscillation spectrum of MISO also differs from SdHO we present the resistivity modulation ΔR_{xx} as a function of B and D at $T = 20$ K in Fig. 2(b). Note, displacement field independent Azbel-Brown-Zak oscillations (ABZO) [27,38] are present in the whole magnetic field range. For comparison, we plot the results of a basic MISO model (see Supplemental Material [20]) using dashed lines that highlight the alignment of Landau levels from different minivalleys. The condition is fulfilled when the energy spacing of an integer number of Landau levels fits the energy offset between the minivalleys, i.e.,

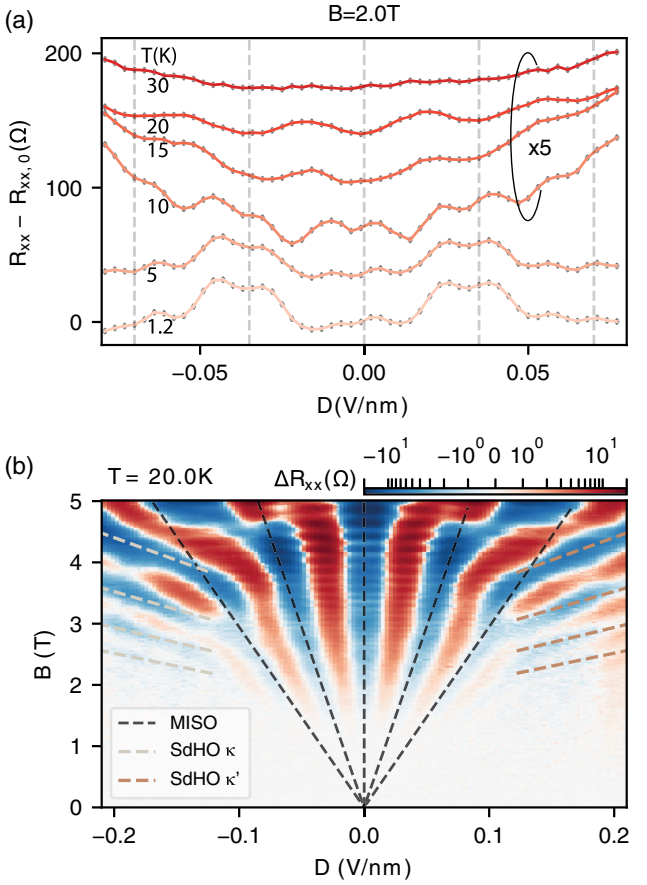

FIG. 2. (a) Line traces of the $R_{xx} - R_{xx,0}$ (value of R_{xx} at $D = 0$) versus displacement field D for various temperatures T as indicated, at constant $n = -2.28 \times 10^{12}$ cm^{-2} and $B = 2$ T. The traces are offset by 35 Ω and the upper four traces are multiplied by 5 for clarity. Vertical dashed lines mark positions of MISO as guides to the eye. (b) Resistance modulation ΔR_{xx} as a function of D and B, taken at $n = -2.28 \times 10^{12}$ cm^{-2} and $T = 20$ K. The black dashed lines represent the result of the basic MISO model, while gray and bronze dashed lines represent SdHO originating from κ and κ' minivalley respectively (see Supplemental Material [20]).

when $\Delta(D) = k\hbar eB/m_{\mathrm{eff}}$ where k is an integer and $m_{\mathrm{eff}} = 0.06m_e$ the effective mass. At $T = 20$ K we estimate that only a few Landau levels participate in transport. The model fits well for moderate D and deviates at higher D, where we suspect the alignment condition is broken because m_{eff} in the minivalleys becomes dissimilar. This is in contrast to semiconductors with mostly parabolic band structure, where larger numbers of Landau levels can overlap at the same time. Finally, we would like to point out the MISO fan in Fig. 2(b) is different from SdHO Landau fans since it has its origin at $D = 0$ [not at finite D as for SdHO in Supplemental Material, Fig. 7], and it fans out in both directions in D.

Generally MISO is considered to be caused by impurity scattering [18]. One would therefore expect to see maxima in the resistivity when the Landau levels from both

minivalleys are aligned. Here, we observed the opposite. Observing minima at MISO resonances indicates that phonon-assisted instead of impurity intersubband scattering is the dominant mechanism [39]. We expect the electron-phonon scattering to be quasielastic, because in Fig. 2(b) the experimentally observed phase of the oscillation matches with the phase of the Landau level alignment in the basic MISO model. Since we observe the MISO resonances as resistance minima in the full temperature range [Fig. 2(a)], we envision scattering by low energy phonons (e.g., flexural phonons) that have a flat dispersion [40,41].

Additionally, we measured the temperature dependence of the resistivity at $B = 0$ and $D = 0$, which shows a linear behavior, indicative of an electron-phonon mechanism. However, since the amplitude of the MISO is small compared to the smooth background [e.g., $\Delta R_{xx}/R_{xx,0} \sim 1\%$ at $T = 20$ K in Fig. 2(a)], the interminivalley scattering is probably not the dominant scattering mechanism determining the resistance. In Supplemental Material [20], apart from a detailed analysis of the temperature dependence of the data, we present a theoretical model that reveals that intraminivalley electron-phonon scattering is likely to be the dominant mechanism.

We continue by analyzing MISO as a function of displacement and magnetic field at $T = 5$ K in Fig. 3(a), focusing on the same density as in Fig. 2(b). The hexagonal pattern is formed by two sets of SdHO originating from respective minivalleys, as indicated in Fig. 3(a), whose discontinuous structure is a result of screening effects. Additionally, displacement field independent ABZO are present throughout the whole magnetic field range. Interestingly, instead of single resistance minima, as observed at the alignment condition of MISO in Fig. 2(b), the MISO resonances are split into two resistance minima at higher magnetic fields, as highlighted by the dark blue arrows in Fig. 3(a), while the SdHO are not split. We extract an effective Landé g factor of $g \approx 5$, pointing toward a splitting of the valley (K and K') degeneracy rather than the spin [42].

The possible Landau level alignments taking into account valley splitting of a single Landau level in each minivalley are schematically shown in Figs. 3(b)–3(d), where three typical energetic offsets are sketched. From this picture one would expect to observe three MISO minima. However, since we only observe two [configurations b and c], the interminivalley scattering must have a valley selection criterion. Note that the MISO splitting is twice that of the Landau levels, which makes it plausible that the splitting is not apparent in the SdHO. In Fig. 3(e) we sketch the mini-Brillouin zones with respective valleys and minivalleys. Considering the relative distance in k space it is more likely that the scattering is valley conserving. In combination with a quasielastic scattering mechanism, this implies that the valley splitting in the two graphene bilayers should be opposite and scattering is only allowed when the same valleys line up, as sketched in Figs. 3(b) and 3(c). Future theoretical work is needed to confirm this possible mechanism.

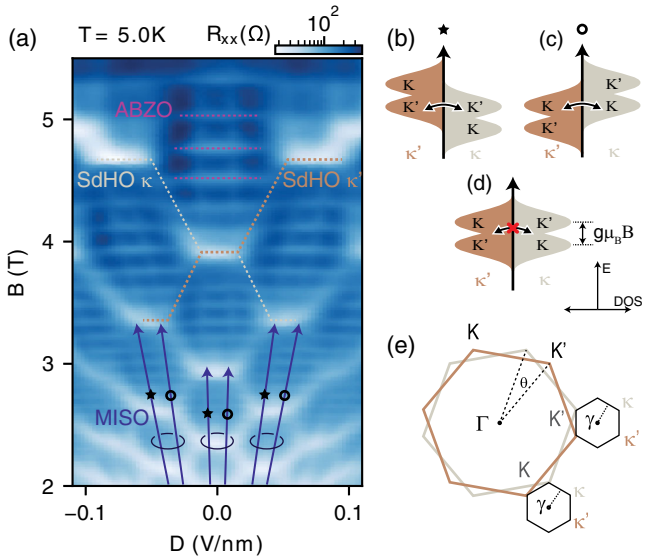

FIG. 3. (a) $R_{xx}(D, B)$ at $T = 5$ K and $n = -2.28 \times 10^{12}$ cm^{-2}. We highlight an example of SdHO from κ and κ' carriers with gray and bronze dashed lines, several ABZO by purple dashed lines, and the split MISO peaks with the dark blue arrows. (b)–(d) Possible description of splitting of the MISO peaks. The density of states (DOS) for both minivalleys κ and κ' are shown for $D < 0$, $D > 0$, and $D = 0$, respectively. The valley splitting and proposed scattering is indicated. (e) Mini-Brillouin zones of TDBG with labeled valleys (K and K') and minivalleys (κ and κ').

After analyzing the region of enhanced MISO in region A of Fig. 1(d), we shift our attention to the region at the onset of the second minivalley occupation, denoted by B in Fig. 1(d). In Fig. 4(a) we plot R_{xx} as a function of B and n, at finite displacement field and temperature of $T = 1.2$ K. At densities below $n \sim -1.5 \times 10^{12}$ cm^{-2}, which is the density onset of the κ minivalley, we measure the Landau fan of κ' minivalley highlighted with bronze dashed lines in Fig. 4(a). Once the Landau levels of the second minivalley appear, the levels in the already occupied κ' minivalley (dotted bronze lines) split as indicated with the bronze arrow in Fig. 4(a), signaling a transition from fourfold to twofold degenerate levels [see also inset of Fig. 4(a)]. To find out which degeneracy (valley or spin) is lifted, we perform additional measurements, using a different cryostat, for two different angles of the magnetic field with respect to the normal of device [see Fig. 4(b)]. Since the splitting depends on $B_\perp$ (and not on $|B|$), we speculate that the valley (K and K') degeneracy in the already occupied κ' minivalley is lifted.

The lifting of the valley degeneracy once the second minivalley gets occupied can be a result of electron-electron interactions, as it is not expected to occur due to single particle effects [43]. A possible electron-electron interaction at play is the valley exchange effect. Furthermore, due to

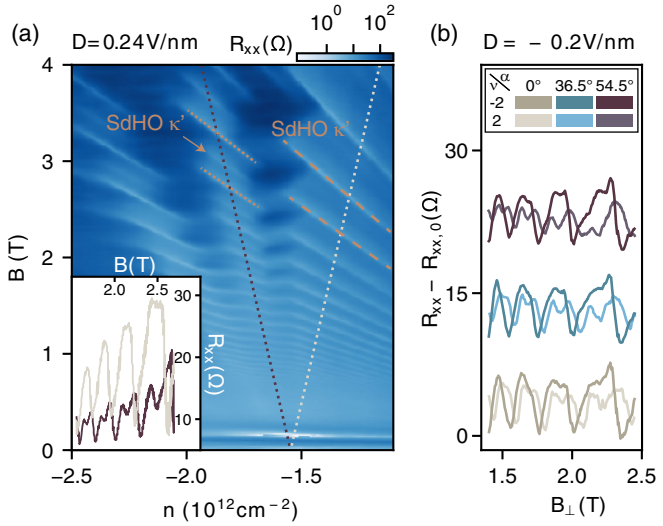

FIG. 4. (a) $R_{xx}(n, B)$ taken at $D = 0.24$ V/nm and $T = 1.2$ K. The inset shows R_{xx} as a function of B, for constant second minivalley filling factors $\nu = \pm 2$ (determined using $m_{\text{eff}} = 0.095 m_e$), as indicated by the dotted lines. (b) $R_{xx} - R_{xx,0}$ taken at $D = -0.2$ V/nm as a function of perpendicular component of the magnetic field $B_\perp$ for $\nu = \pm 2$ and $\alpha = 0°$, 36.5°, 54.5°.

high effective mass at the onset of the second minivalley, screening effects can improve the mobility leading to better linewidth of SdHO hence revealing the splitting in the spectrum. However, since we observe enhanced MISO, i.e., stronger scattering, at the onset of the second minivalley, we speculate that the observed enhanced interminivalley scattering leading to MISO in region B of Fig. 1(d) is due to an electron-electron scattering mechanism.

In summary, by using MISO as a targeted measurement approach, we have investigated interminivalley scattering in a moiré material. We found two regions of enhanced MISO, and discussed the likely scattering mechanisms of electron-phonon scattering with a valley selection rule in the vicinity of the Lifshitz transition and electron-electron scattering at the onset of the second minivalley. The described measurement technique is transferable to other moiré materials [44,45], given that they adhere to the prerequisites of a clear Landau level spectrum and sufficient tunability. Furthermore, when decreasing the twist angle the regions of enhanced MISO merge, the minivalleys come closer in k space, and the effective mass is lowered further as the bands become flatter. We therefore anticipate interminivalley scattering to increase strongly. Our observations may give a handle to refine theoretical models that aim to capture interactions in moiré systems, such as magic-angle twisted bilayer graphene.

All data used in this Letter are made available online [46].

We acknowledge the support from Peter Maerki, Thomas Baehler, and the staff of the ETH FIRST cleanroom facility.

We acknowledge support from the Graphene Flagship, the Swiss National Science Foundation via NCCR Quantum Science and from the European Union's Horizon 2020 research and innovation programme under Grant No. 862660/QUANTUM E LEAPS. P. T. acknowledges funding through the NCCR SPIN. E. P. acknowledges support of a fellowship from la Caixa Foundation (ID 100010434) under fellowship code LCF/BQ/EU19/11710062. K. W. and T. T. acknowledge support from the Elemental Strategy Initiative conducted by the MEXT, Japan, Grant No. JPMXP0112101001, JSPS KAKENHI Grant No. JP20H00354, and the CREST (JPMJCR15F3), JST.

Note added.—Recently, we became aware of a complementary work [45] in twisted bilayer graphene.

*ptomic@phys.ethz.ch
†devriesf@phys.ethz.ch

[1] A. H. Castro Neto, F. Guinea, N. M. R. Peres, K. S. Novoselov, and A. K. Geim, The electronic properties of graphene, Rev. Mod. Phys. **81**, 109 (2009).
[2] M. Kuwabara, D. R. Clarke, and D. A. Smith, Anomalous superperiodicity in scanning tunneling microscope images of graphite, Appl. Phys. Lett. **56**, 2396 (1990).
[3] R. Bistritzer and A. H. MacDonald, Moiré bands in twisted double-layer graphene, Proc. Natl. Acad. Sci. U.S.A. **108**, 12233 (2011).
[4] Y. Cao, V. Fatemi, A. Demir, S. Fang, S. L. Tomarken, J. Y. Luo, J. D. Sanchez-Yamagishi, K. Watanabe, T. Taniguchi, E. Kaxiras, R. C. Ashoori, and P. Jarillo-Herrero, Correlated insulator behaviour at half-filling in magic-angle graphene superlattices, Nature (London) **556**, 80 (2018).
[5] Y. Cao, V. Fatemi, S. Fang, K. Watanabe, T. Taniguchi, E. Kaxiras, and P. Jarillo-Herrero, Unconventional superconductivity in magic-angle graphene superlattices, Nature (London) **556**, 43 (2018).
[6] A. L. Sharpe, E. J. Fox, A. W. Barnard, J. Finney, K. Watanabe, T. Taniguchi, M. A. Kastner, and D. Goldhaber-Gordon, Emergent ferromagnetism near three-quarters filling in twisted bilayer graphene, Science **365**, 605 (2019).
[7] X. Lu, P. Stepanov, W. Yang, M. Xie, M. A. Aamir, I. Das, C. Urgell, K. Watanabe, T. Taniguchi, G. Zhang, A. Bachtold, A. H. MacDonald, and D. K. Efetov, Superconductors, orbital magnets and correlated states in magic-angle bilayer graphene, Nature (London) **574**, 653 (2019).
[8] G. W. Burg, J. Zhu, T. Taniguchi, K. Watanabe, A. H. MacDonald, and E. Tutuc, Correlated Insulating States in Twisted Double Bilayer Graphene, Phys. Rev. Lett. **123**, 197702 (2019).
[9] Y. Cao, D. Rodan-Legrain, O. Rubies-Bigorda, J. M. Park, K. Watanabe, T. Taniguchi, and P. Jarillo-Herrero, Tunable correlated states and spin-polarized phases in twisted bilayer–bilayer graphene, Nature (London) **583**, 215 (2020).
[10] P. Rickhaus, F. K. de Vries, J. Zhu, E. Portolés, G. Zheng, M. Masseroni, A. Kurzmann, T. Taniguchi, K. Wantanabe,

A. H. MacDonald, T. Ihn, and K. Ensslin, Density-wave states in twisted double-bilayer graphene, Science **373**, 1257 (2021).
[11] F. K. de Vries, J. Zhu, E. Portolés, G. Zheng, M. Masseroni, A. Kurzmann, T. Taniguchi, K. Watanabe, A. H. MacDonald, K. Ensslin, T. Ihn, and P. Rickhaus, Combined Minivalley and Layer Control in Twisted Double Bilayer Graphene, Phys. Rev. Lett. **125**, 176801 (2020).
[12] K. I. Bolotin, K. J. Sikes, J. Hone, H. L. Stormer, and P. Kim, Temperature-Dependent Transport in Suspended Graphene, Phys. Rev. Lett. **101**, 096802 (2008).
[13] H. Polshyn, M. Yankowitz, S. Chen, Y. Zhang, K. Watanabe, T. Taniguchi, C. R. Dean, and A. F. Young, Large linear-in-temperature resistivity in twisted bilayer graphene, Nat. Phys. **15**, 1011 (2019).
[14] F. Wu, E. Hwang, and S. Das Sarma, Phonon-induced giant linear-in-t resistivity in magic angle twisted bilayer graphene: Ordinary strangeness and exotic superconductivity, Phys. Rev. B **99**, 165112 (2019).
[15] Y. Cao, D. Chowdhury, D. Rodan-Legrain, O. Rubies-Bigorda, K. Watanabe, T. Taniguchi, T. Senthil, and P. Jarillo-Herrero, Strange Metal in Magic-Angle Graphene with Near Planckian Dissipation, Phys. Rev. Lett. **124**, 076801 (2020).
[16] E. H. Hwang and S. Das Sarma, Linear-in-T resistivity in dilute metals: A Fermi liquid perspective, Phys. Rev. B **99**, 085105 (2019).
[17] V. M. Polyanovskii, Anomalous temperature-dependence of the amplitude of quantum oscillations of the magnetoresistance in quasi-two-dimensional systems, Fiz. Tekh. Poluprovodn. **22**, 2230 (1988) [Sov. Phys. Semicond. **22**, 1408 (1988)].
[18] I. A. Dmitriev, A. D. Mirlin, D. G. Polyakov, and M. A. Zudov, Nonequilibrium phenomena in high Landau levels, Rev. Mod. Phys. **84**, 1709 (2012).
[19] I. M. Lifshitz, Anomalies of electron characteristics of a metal in the high pressure region, Zh. Eksp. Teor. Fiz. **38**, 1569 (1960) [Sov. Phys. JETP **11**, 1130 (1960)].
[20] See Supplemental Material at http://link.aps.org/supplemental/10.1103/PhysRevLett.128.057702 for details on the band structure calculations, the device fabrication, data analysis, capacitor models, and temperature dependent resistivity measurements, which includes Refs. [3,21–37].
[21] J. C. Slonczewski and P. R. Weiss, Band structure of graphite, Phys. Rev. **109**, 272 (1958).
[22] J. W. McClure, Band structure of graphite and de Haas–van Alphen effect, Phys. Rev. **108**, 612 (1957).
[23] J. W. McClure, Theory of diamagnetism of graphite, Phys. Rev. **119**, 606 (1960).
[24] J. M. B. Lopes dos Santos, N. M. R. Peres, and A. H. Castro Neto, Graphene Bilayer with a Twist: Electronic Structure, Phys. Rev. Lett. **99**, 256802 (2007).
[25] A. B. Kuzmenko, I. Crassee, D. van der Marel, P. Blake, and K. S. Novoselov, Determination of the gate-tunable band gap and tight-binding parameters in bilayer graphene using infrared spectroscopy, Phys. Rev. B **80**, 165406 (2009).
[26] S. Slizovskiy, A. Garcia-Ruiz, N. Drummond, and V. I. Falko, Dielectric susceptibility of graphene describing its out-of-plane polarizability, Nano Lett. **21**, 6678 (2021).
[27] F. K. de Vries *et al.*, Phase coherent magnetotransport along a network of critical trajectories near Lifshitz transition (to be published).
[28] P. Rickhaus, M.-H. Liu, M. Kurpas, A. Kurzmann, Y. Lee, H. Overweg, M. Eich, R. Pisoni, T. Taniguchi, K. Watanabe *et al.*, The electronic thickness of graphene, Sci. Adv. **6**, eaay8409 (2020).
[29] T. Ihn, *Semiconductor Nanostructures: Quantum States and Electronic Transport* (Oxford University Press, New York, 2010).
[30] A. Savitzky and M. J. Golay, Smoothing and differentiation of data by simplified least squares procedures, Anal. Chem. **36**, 1627 (1964).
[31] F. Bloch, Zum elektrischen widerstandsgesetz bei tiefen temperaturen, Z. Phys. **59**, 208 (1930).
[32] E. Grüneisen, Die abhängigkeit des elektrischen widerstandes reiner metalle von der temperatur, Ann. Phys. (Berlin) **408**, 530 (1933).
[33] A. Garcia-Ruiz, H. Deng, V. V. Enaldiev, and V. I. Fal'ko, Full Slonczewski-Weiss-McClure parametrization of few-layer twistronic graphene, Phys. Rev. B **104**, 085402 (2021).
[34] X. Cong, Q.-Q. Li, X. Zhang, M.-L. Lin, J.-B. Wu, X.-L. Liu, P. Venezuela, and P.-H. Tan, Probing the acoustic phonon dispersion and sound velocity of graphene by Raman spectroscopy, Carbon **149**, 19 (2019).
[35] J. R. Wallbank, R. Krishna Kumar, M. Holwill, Z. Wang, G. H. Auton, J. Birkbeck, A. Mishchenko, L. A. Ponomarenko, K. Watanabe, T. Taniguchi, K. S. Novoselov, I. L. Aleiner, A. K. Geim, and V. I. Fal'ko, Excess resistivity in graphene superlattices caused by umklapp electron-electron scattering, Nat. Phys. **15**, 32 (2019).
[36] L. Landau and E. Lifshitz, *Physical Kinetics: Theoretical Physics Course* (Butterworth-Heinemann, Oxford, 1980), Vol. 10.
[37] J. M. Ziman, *Electrons and Phonons: The Theory of Transport Phenomena in Solids* (Oxford University Press, New York, 1960).
[38] R. Krishna Kumar, X. Chen, G. H. Auton, A. Mishchenko, D. A. Bandurin, S. V. Morozov, Y. Cao, E. Khestanova, M. Ben Shalom, A. V. Kretinin, K. S. Novoselov, L. Eaves, I. V. Grigorieva, L. A. Ponomarenko, V. I. Fal'ko, and A. K. Geim, High-temperature quantum oscillations caused by recurring Bloch states in graphene superlattices, Science **357**, 181 (2017).
[39] O. E. Raichev, Magnetoresistance oscillations in two-subband electron systems: Influence of electron-phonon interaction, Phys. Rev. B **81**, 195301 (2010).
[40] M. Koshino and Y.-W. Son, Moiré phonons in twisted bilayer graphene, Phys. Rev. B **100**, 075416 (2019).
[41] A. I. Cocemasov, D. L. Nika, and A. A. Balandin, Phonons in twisted bilayer graphene, Phys. Rev. B **88**, 035428 (2013).
[42] Y. Lee, A. Knothe, H. Overweg, M. Eich, C. Gold, A. Kurzmann, V. Klasovika, T. Taniguchi, K. Wantanabe, V. Fal'ko, T. Ihn, K. Ensslin, and P. Rickhaus, Tunable Valley Splitting due to Topological Orbital Magnetic Moment in Bilayer Graphene Quantum Point Contacts, Phys. Rev. Lett. **124**, 126802 (2020).
[43] J. A. Crosse, N. Nakatsuji, M. Koshino, and P. Moon, Hofstadter butterfly and the quantum Hall effect in

twisted double bilayer graphene, Phys. Rev. B **102**, 035421 (2020).

[44] M. Masseroni, T. Davatz, R. Pisoni, F. K. de Vries, P. Rickhaus, T. Taniguchi, K. Watanabe, V. Fal'ko, T. Ihn, and K. Ensslin, Electron transport in dual-gated three-layer MoS_2, Phys. Rev. Research **3**, 023047 (2021).

[45] I. Y. Phinney, D. A. Bandurin, C. Collignon, I. A. Dmitriev, T. Taniguchi, K. Watanabe, and P. Jarillo-Herrero, Strong Interminivalley Scattering in Twisted Bilayer Graphene Revealed by High-Temperature Magneto-Oscillations, Phys. Rev. Lett. **127**, 056802 (2021).

[46] ETH Zürich research collection (2021), 10.3929/ethz-b-000508511.